Rotor Position Self-Sensing of SRM Using PSO-RVM

Qianwen Xiang (ID), **Ye Yuan *, Yanjun Yu and Kunhua Chen**

School of Electrical and Information Engineering, Jiangsu University, Zhenjiang 212013, China;
xqw@ujs.edu.cn (Q.X.); yuyanjun@ujs.edu.cn (Y.Y.); chenkunhua@ujs.edu.cn (K.C.)
* Correspondence: 1000050003@ujs.edu.cn; Tel.: +86-13952857037

Abstract: The motors' flux-linkage, current and angle obtained from the system with sensors were chosen as the sample data, and the estimation model of rotor position based on relevance vector machine (RVM) was built by training the sample data. The kernel function parameter in RVM model was optimized by the particle swarm algorithm in order to increase the fitting precision and generalization ability of RVM model. It achieved higher prediction accuracy with staying at the same on-line testing time as the RVM. And because the short on-line computation, the motor can operate at 3000 r/min in sensorless control with particle swarm optimization-relevance vector machine (PSO-RVM), which is higher than support vector machine (SVM) and neural network (NN). By simulation and experiment on the test motor, it is verified that the proposed estimation model can obtain the angle of full electrical period accurately under low speed and high speed operations in current chopped control and angle position control, which has satisfactory estimation precision.

Keywords: relevance vector machine (RVM); particle swarm; switched reluctance motor; estimation model; self-sensing

1. Introduction

Switched reluctance motor (SRM) is widely used in many fields, such as hauling, aircraft, mining and textile industries, because of its high efficiency, low cost, simple mechanism, great reliability and wide regulating range. Generally, SRM under position closed-loop speed control is equipped with a position sensor to directly measure rotor position signals. However, mechanical sensor not only has raised the system cost and complexity, but also has affected the overall reliability of the SRM drive system [1]. Therefore, both domestic and foreign researchers have spent considerable time and efforts exploring the SRM rotor position self-sensing technology. However, the nonlinear flux-linkage characteristics of switched reluctance motor make it difficult to detect the rotor position.

A large number of methods for the rotor position self-sensing of switched reluctance motors are studied in recent years. In [2], a linear frequency modulated converter is used to measure inductance, whose output is decoded to get the rotor angle. But because the detection signal is easily disturbed, this method has low precision. In [3], a single high-frequency pulse is injected in the non-conducting phase to estimate the rotor angle, which neglects the influence of the back electromotive force (EMF) and the winding equivalent voltage and has estimation precision influenced by speed. In [4,5], the observer-based method is used to obtain the rotor angle of full electrical period. However, the observer relies on more complex mathematical models, and the algorithm is complex and difficult to be widely used. In [6], a look-up table with flux linkage, current and angle is proposed to estimating continuous rotor position, but it has a long look-up time and requires large memory. In [7,8], improved simplified flux method with flux-linkage and current at the maximum inductance position is presented, which has less memory and shorter computing time. However, all these methods about look-up table require chopped current control, not fit for angle position control. In all the methods, the flux-linkage

is used most in the rotor position self-sensing because it is the fundamental characteristic of SRM. So many studies are focused on obtain accurate flux-linkage characteristic in SRM sensorless control.

In [9–15], neural network (NN) and support vector machine (SVM) are used to predict rotor position of SRM, some achievements have been acquired. But the NN prediction process takes up a lot of resources and has long training time, and there are some defects such as local minimum, over fitting. With the increase of training samples, the training time becomes longer with the SVM, and the adaptive ability is poor and the robustness is not strong. Because of the long online decision-making time, the position sensorless SRM based on the NN and SVM methods proposed in the above-mentioned studies works at the maximal rotational speed of 1500 r/min only.

Relevance vector machine (RVM) is a non-linear probability model [16,17] put forward by Tipping. Compared to SVM, RVM uses Bayesian methods for reasoning where the kernel function is not necessarily required to fulfill Mercer's condition—which consequently widen the range of eligible kernel function; more importantly, because the model parameters (relevance vectors) slowly increase as the sample size grows, there are sparser solutions while the model is less complex and the time of decision making is shorter. Thus, RVM is more suitable for the scenarios requiring real-time results. When it is used in rotor position self-sensing, SRM can operate at a higher speed compared to the NN and SVM.

Despite RVM's advantages, its performance depends on the optimum selection of parameters of kernel function and yet, there are no unified optimum standards [18]. The commonly methods used mesh parameterization require a large amount of computation and long-time searching; besides, the least square method is largely restricted by the initial iterative value. Hence, it is likely to result in locally optimal solutions. In recent years, the particle swarm optimization (PSO) algorithm [19] and the genetic algorithm (GA) [20] have been employed to optimize the parameters of RVM's kernel function, which have effectively reduced the time of searching and the dependence on the initial iterative value. The PSO algorithm and the GA are both optimization algorithms based on the swarm and adaptation concepts, with the difference between the two lying in that the PSO algorithm enables memorization of optimal particle positions and inter particle information sharing mechanism whereas GA involves complicated genetic operations, such as selection, crossing-over, variation and so on. The former algorithm has the advantage over the latter in convergence, rule setting and implementation. Therefore, in this paper, the PSO algorithm was used for the optimization of RVM parameters.

To fulfill the real-time requirements for rotor position self-sensing, this paper presented an RVM-based SRM rotor position estimation method. From SRM's non-linear flux-linkage characteristic, an RVM-based rotor position estimation model was built through sampled data training. Considering that the kernel function parameters of the RVM model were difficult to determine, the PSO algorithm was introduced to optimize the parameters of the RVM model to further improve the model's precision of estimation. It proved that the PSO-RVM model has a higher prediction precision, a shorter on-line testing time than the RVM and SVM model by the simulation. The experiment results show that the motor can operate at 1500 r/min and 3000 r/min steadily in sensorless control.

2. Flux-Linkage Characteristic of SRM

SRM is a brushless stator-rotor double salient pole variable reluctance machine, of which the flux-linkage shows time-dependent unidirectional pulse changes while the air-gap field is of pulsation. The non-linear geometric structure and magnetic circuit make SRM's single-phase winding flux-linkage ψ a non-linear function of the phase winding current i and the rotor position angle θ:

$$\psi = \psi(i, \theta) \tag{1}$$

It can be proved that the equation above has a unique uniform reciprocal function [9]:

$$\theta = \theta(\psi, i) \tag{2}$$

Such that θ at a time can be calculated according to the known ψ and i at the such time. As to a three-phase 12/8 SRM, assumed the stator pole and the rotor pole in an aligned position, i.e., $\theta = 0°$, and the stator pole and the rotor slot in an aligned position, i.e., $\theta = 22.5°$, according to the symmetry of the SRM structure, the motor's magnetic characteristic can be reflected by measuring the flux-linkage value of the rotor in the semi-cycle ranging from 0–22.5°, as shown in Figure 1. It can be seen that: (1) As the excitation current becomes stronger, the rotor position angle decreases, the stator and the rotor gradually align with each other, the magnetic field reaches the state of saturation and the growth of flux-linkage turns increasingly slow in a non-linear manner; (2) There are unique mapping relationships among flux-linkage, phase current and rotor position angle.
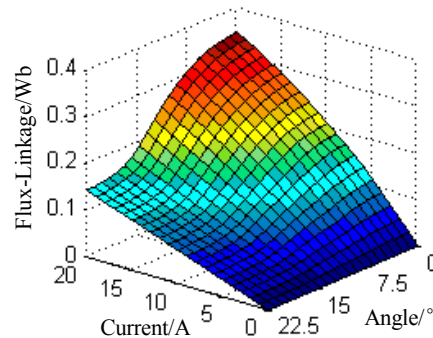
Figure 1. Switched reluctance motor (SRM) flux-linkage character.

3. RVM-Based Regression Modeling with PSO Algorithm

Considering SRM's non-linear magnetic characteristic, only simplified model of magnetic linkage can be built through regular modeling by mechanism. If the running parameters and status of the SRM system change, the simplified model will bring lower precision, in which case, the precision of using the simplified model for rotor position estimation will decrease accordingly. To prevent model bias and parameter uncertainties that may influence the rotor position estimation model and to improve the precision and self-adaptation of rotor position estimation, in this paper, RVM's universal approximation of any functions was utilized to identify the SRM rotor position angle.

3.1. RVM Regression Modeling

Given that the input vector set and output vector set of the training samples are $\{\mathbf{x}_i | i = 1, \ldots, N\}$ and $\{\mathbf{y}_i | i = 1, \ldots, N\}$ respectively, the objective function y_i is defined to be derived from a model with noise:

$$y_i = \sum_{i=1}^{N} \omega_i K(\mathbf{x}, \mathbf{x}_i) + \omega_0 + \varepsilon_i \tag{3}$$

where the noise ε_i is subject to the Gaussian distribution with the mean as zero and the variance as σ^2; $\boldsymbol{\omega} = (\omega_0, \ldots, \omega_N)^{\mathrm{T}}$ represents the weight vector; $K(\mathbf{x}, \mathbf{x}_i)$ expresses the kernel function (not necessarily to satisfy Mercer's condition). The likelihood function of the training sample set can be described as:

$$p(\mathbf{y}|\boldsymbol{\omega}, \sigma^2) = (2\pi\sigma^2)^{-\frac{N}{2}} \exp\left(-\frac{\|\mathbf{y} - \boldsymbol{\Phi}\boldsymbol{\omega}\|^2}{2\sigma^2}\right) \tag{4}$$

where $\mathbf{y} = [y_1, \ldots, y_N]^{\mathrm{T}}$; $\boldsymbol{\Phi}$ means the basis function matrix that can be expressed by:

$$\mathbf{\Phi} = \begin{bmatrix} 1 & K(\mathbf{x}_1, \mathbf{x}_1) & \cdots & K(\mathbf{x}_1, \mathbf{x}_N) \\ 1 & K(\mathbf{x}_2, \mathbf{x}_1) & \cdots & K(\mathbf{x}_2, \mathbf{x}_N) \\ \vdots & \vdots & & \vdots \\ 1 & K(\mathbf{x}_N, \mathbf{x}_1) & \ldots & K(\mathbf{x}_N, \mathbf{x}_N) \end{bmatrix} \tag{5}$$

The Gaussian framework was employed to generalize the RVM regression model. The prior distribution of parameters is defined as:

$$p(\boldsymbol{\omega}|\boldsymbol{\alpha}) = (2\pi)^{-\frac{N}{2}} \prod_{i=0}^{N} \alpha_i^{\frac{1}{2}} \exp\left(-\frac{\alpha_i \omega_i^2}{2}\right) \tag{6}$$

where $\boldsymbol{\alpha} = [\alpha_0, \ldots, \alpha_N]$ is a hyper-parameter.

Based on the prior distribution and plausible reasoning distribution, the posterior distribution of weight can be known through Bayesian inference. The posterior distribution can be expressed by:

$$p(\boldsymbol{\omega}|\mathbf{y}, \boldsymbol{\alpha}, \sigma^2) = \frac{p(\mathbf{y}|\boldsymbol{\omega}, \sigma^2) p(\boldsymbol{\omega}|\boldsymbol{\alpha})}{p(\mathbf{y}|\boldsymbol{\alpha}, \sigma^2)} = (2\pi)^{-\frac{N+1}{2}} |\mathbf{R}|^{-\frac{1}{2}} \exp\left\{-\frac{1}{2}(\boldsymbol{\omega} - \boldsymbol{\mu})^T \mathbf{R}^{-1}(\boldsymbol{\omega} - \boldsymbol{\mu})\right\} \tag{7}$$

where the posterior covariance can be represented by:

$$\mathbf{R} = (\sigma^{-2} \mathbf{\Phi}^T \mathbf{\Phi} + \mathbf{A})^{-1} \tag{8}$$

The posterior mean can be described as:

$$\boldsymbol{\mu} = \sigma^{-2} \mathbf{R} \mathbf{\Phi}^T \mathbf{t} \tag{9}$$

where $\mathbf{A} = \mathrm{diag}(\alpha_0, \ldots, \alpha_N)$.

The equation of likelihood function (4) of sample set training was used for integration of weight variables and the $\boldsymbol{\alpha}$ and σ^2-dependent marginal distribution of plausible values can be described as:

$$p(\mathbf{y}|\boldsymbol{\alpha}, \sigma^2) = (2\pi)^{-\frac{N}{2}} |\mathbf{\Omega}|^{-\frac{1}{2}} \exp\left(-\frac{\mathbf{y}^T \mathbf{\Omega}^{-1} \mathbf{y}}{2}\right) \tag{10}$$

where $\mathbf{\Omega} = \sigma^2 \mathbf{I} + \mathbf{\Phi} \mathbf{A}^{-1} \mathbf{\Phi}^T$; $\mathbf{I}$ represents an n-order unit matrix.

Because the maximum $\boldsymbol{\alpha}$ and σ^2 cannot be obtained by Equation (10) with the analytical method, iterative estimation was adopted. Taking a derivative of $\boldsymbol{\alpha}$ based on Equation (10) to make $\boldsymbol{\alpha}$ to zero, the updated value of α_i can be expressed by:

$$\alpha_{i,\mathrm{new}} = \frac{\gamma_i}{\mu_i^2} \tag{11}$$

where $\gamma_i = 1 - \alpha_i R_{ii}$, R_{ii} is the ith diagonal element of the posterior weight covariance matrix $\mathbf{R}$, the calculation result of the known $\boldsymbol{\alpha}$ and σ^2 according to Equation (8); μ_i denotes the ith posterior mean that can be calculated based on Equation (9).

Taking the above-mentioned method to take a derivative of μ_i, the equation can be rewritten as:

$$\sigma_{\mathrm{new}}^2 = \frac{\|\mathbf{y} - \mathbf{\Phi}\mu\|^2}{N - \sum\limits_{i=1}^{N} \gamma_i} \tag{12}$$

Knowing the parameters $\alpha_{i,\mathrm{new}}$ and σ_{new}^2, the weighted posterior mean and variance were recalculated. During iteration, most of α_i tend to approach infinity, indicating that the corresponding

ω_i values equal zero. In this case, the corresponding basis function can be deleted to achieve sparsity. When other α_i values approach infinity in a steady manner, the corresponding $\mathbf{x}_i$ is defined as a relevance vector.

In RVM regression modeling, Gaussian kernel function $K(\mathbf{x}, \mathbf{x}_i) = \exp\left(\frac{-\|\mathbf{x}-\mathbf{x}_i\|^2}{2\delta^2}\right)$ was applied to the high-dimensional mapping in this study. The RVM regression model can be rewritten as:

$$y_i = \sum_{i=1}^{N} \omega_i \exp\left(\frac{-\|\mathbf{x}-\mathbf{x}_i\|^2}{2\delta^2}\right) + \omega_0 \tag{13}$$

where δ represents the width of the Gaussian kernel function that reflects the radius of the closed boundary.

3.2. PSO-RVM Model Parameters

The PSO algorithm is an iterative optimization algorithm which is first proposed by Kennedy and Eberhart in 1995. This algorithm is a simulation of social behavior of birds, which is an optimization algorithm based on group (population), similar to GA. Each particle adjusts its evolutionary direction through information interaction with other particles, and avoids falling into local optimum. In addition, PSO algorithm adopts random search strategy different from GA, which is much simpler than GA. Therefore, it shows better performance when solving some optimization problems.

According to Equation (13), when the training samples are determined, the generalization and estimation precision of the RVM regression model depend on the parameter δ^2 of the kernel function and yet, there is no unified principle regarding the selection of δ^2 [13]. Therefore, this paper utilized the global searching function of the PSO algorithm to optimize the kernel function parameter δ^2 and improve the generalization and estimation performance of RVM.

In a complex m-D space, the PSO algorithm implements searching through loop iteration. In each loop, the velocity and position of particle i are updated by dynamic tracking of its optimal value $p_{\text{best}} = \{p_{i1}, p_{i2}, \cdots, p_{im}\}$ and that of the swarm $g_{\text{best}} = \{g_1, g_2, \cdots, g_m\}$. Assumed that $v_i = \{v_{i1}, v_{i2}, \cdots, v_{im}\}$ and $x_i = \{x_{i1}, x_{i2}, \cdots, x_{im}\}$ are respectively the velocity and position of particle i, v_i and x_i can be updated according to the equations as follows:

$$v_i^{k+1} = \omega v_i^k + c_1 r(\cdot)(p_{\text{best}} - x_i^k) + c_2 r(\cdot)(g_{\text{best}} - x_i^k) \tag{14}$$

$$x_i^{k+1} = x_i^k + v_i^{k+1} \tag{15}$$

$$-v_{\max} < v_i^{k+1} < v_{\max} \tag{16}$$

where k means the number of iterations, ω means the inertia weight coefficient, $r(\cdot)$ expresses a random value between (0, 1) and c_1 and c_2 denote learning factors. $v_{\max}$ is the predetermined maximum velocity.

The application of the foregoing PSO algorithm to the optimization of the RVM model parameter δ^2 is as shown in Figure 2.

In the iteration process, the fitness function is defined as:

$$f(\delta^2) = \frac{\sum\limits_{i=1}^{N} \text{Inv}(\text{abs}(y_i - y))}{N}, i = 1, 2, \ldots, N \tag{17}$$

where $y_i = \sum\limits_{i=1}^{N} \omega_i \exp\left(\frac{-\|\mathbf{x}-\mathbf{x}_i\|^2}{2\delta^2}\right) + \omega_0$ is the predictive value given by the RVM model while y is the actual value.

The suspensive condition of the iterative algorithm is $k \geq k_{\max}$ or $f(\delta^2) \leq f_{\min}$, where $k_{\max}$ means the maximum number of iteration and $f_{\min}$ represents the minimum adaptive threshold.
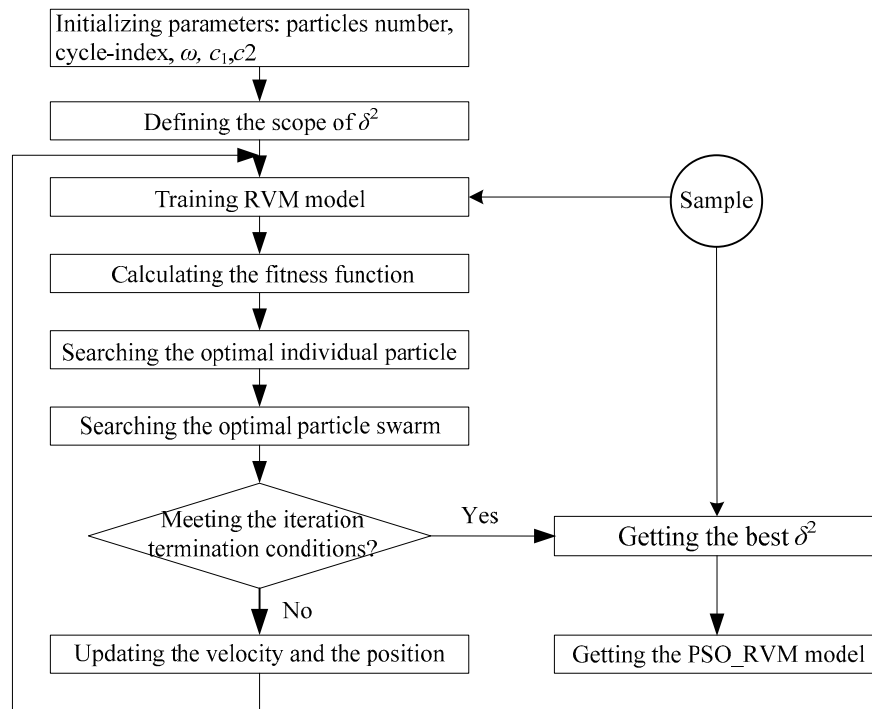
Figure 2. The flowchart of particle swarm optimization-relevance vector machine (PSO-RVM).

4. PSO-RVM-Based SRM Rotor Position Self-Sensing

According to Equation (2), i and ψ are inputs of PSO-RVM learning while the corresponding θ is the output. With a limited number of learning samples, the PSO-RVM after learning can reflect the non-linear functional relations and estimate the rotor position.

First, the SRM experiment system was used for sampling to fetch learning samples. Specifically, the phase current and rotor position can be directly detected with sensors while the phase flux-linkage can be indirectly obtained through phase voltage and phase current sampling.

The jth phase winding voltage loop equation of SRM can be described as:

$$u_j = i_j r + \frac{d\psi_j}{dt} \tag{18}$$

where u_j, i_j and ψ_j respectively represent the voltage, current and flux-linkage of the jth phase and r denotes the phase winding resistance. Based on Equation (17), the flux-linkage can be expressed by:

$$\psi_j = \int_0^t (u_j - i_j r)dt + \psi_j(0) \tag{19}$$

where $\psi_j(0)$ means the initial flux-linkage value. The flux-linkage in the discrete sampling control system can be described as:

$$\psi_j(k) = \psi_j(k-1) + 0.5\text{T}\big[u_j(k) - ri_j(k) + u_j(k-1) - ri_j(k-1)\big] \tag{20}$$

where $\psi_j(k)$ and $\psi_j(k-1)$ denote the flux-linkage values of the kth and the $k-1$th sampling respectively; $u_j(k)$, $u_j(k-1)$, $i_j(k)$, $i_j(k-1)$ are the corresponding voltage, detected current of the kth and the $k-1$th sampling; T represents the sampling time.

Then, according to the algorithm flow as shown in Figure 2, the software Matlab was applied to PSO-RVM training in order to obtain the optimal kernel function parameter $\delta_{\max}$ best and relevance vector and build a PSO-RVM model for SRM rotor position estimation as shown in Figure 3, where:

The input variable can be expressed by: $\mathbf{x}_j = [\psi_j, i_j]^{\mathrm{T}}$.

The Gaussian kernel function after optimizing the kernel width with the PSO algorithm can be described as: $K(\mathbf{x}, \mathbf{x}_i) = \exp\left(\frac{-\|\mathbf{x}-\mathbf{x}_i\|^2}{2\delta_{\text{best}}^2}\right) (i = 1, 2, \ldots, N)$.

The output variable can be defined as: $y_j = \hat{\theta}_j = \sum\limits_{i=1}^{N} \omega_i K(\mathbf{x}, \mathbf{x}_i) + \omega_0$.
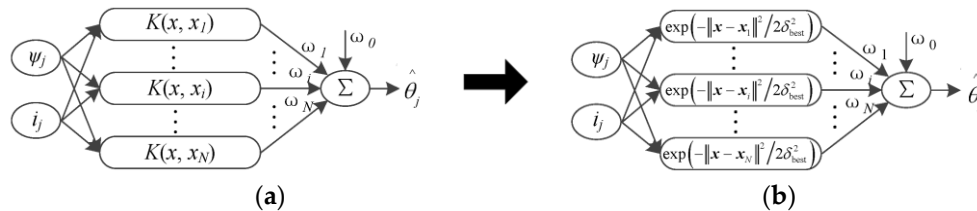
Figure 3. The model structure of relevance vector machine (RVM) and PSO-RVM. (**a**) The RVM structure; (**b**) The PSO-RVM structure.

Lastly, the PSO-RVM-based estimation model that was built offline was applied to real-time control. The real-time phase current and phase voltage were detected with sensors while the flux-linkage was calculated according to Equation (20). Subsequently, the current and flux-linkage values were input into the PSO-RVM-based rotor position prediction model to calculate the rotor position at the exact time point and ultimately realize SRM rotor position self-sensing.

5. Simulation and Experiment

5.1. Self-Sensing Control Algorithm

The rotor self-sensing control system is built by Matlab as shown in Figure 4. The PSO-RVM estimator calculates the output ψ by the input i and θ. The commutation controller calculates the duty cycle according to calculated θ and reference value θ_{on} and θ_{off}. The PWM signals are generated by the duty cycle controller. The current controller generates chopping current signals according to the tested i and the speed error. The power converters generate driving signal of each phase winding according to the chopping signals and PWM signals.
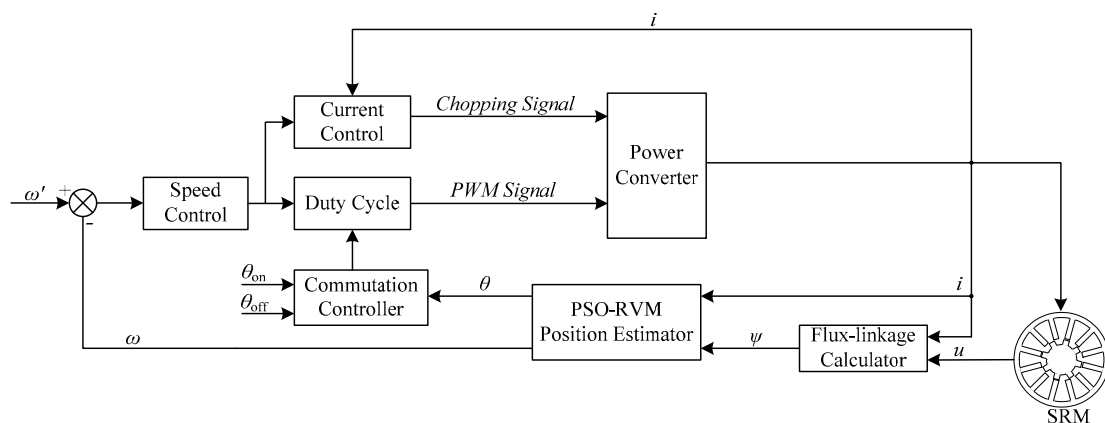
Figure 4. Simulation diagram of rotor position self-sensing.

Flowchart of the control algorithm is shown in Figure 5. The first initial phase is chosen by detect the phase current i. The phase voltage u and i are sampled to calculate the ψ and estimate θ by setting the main timer (Timer 1). When the estimate θ is near the setting θ, the θ_{on} and θ_{off} are captured by setting another timer (Timer 2). In order to avoid overcurrent, the sampled i and the referenced i

are compared. The estimated ω is calculated in every electrified cycle 45° and the referenced ω is −30°. As ω changes, the setting of the Timer 1 is also changed. Usually, when ω increases, the Timer 1 interrupt period will get shorter [12].
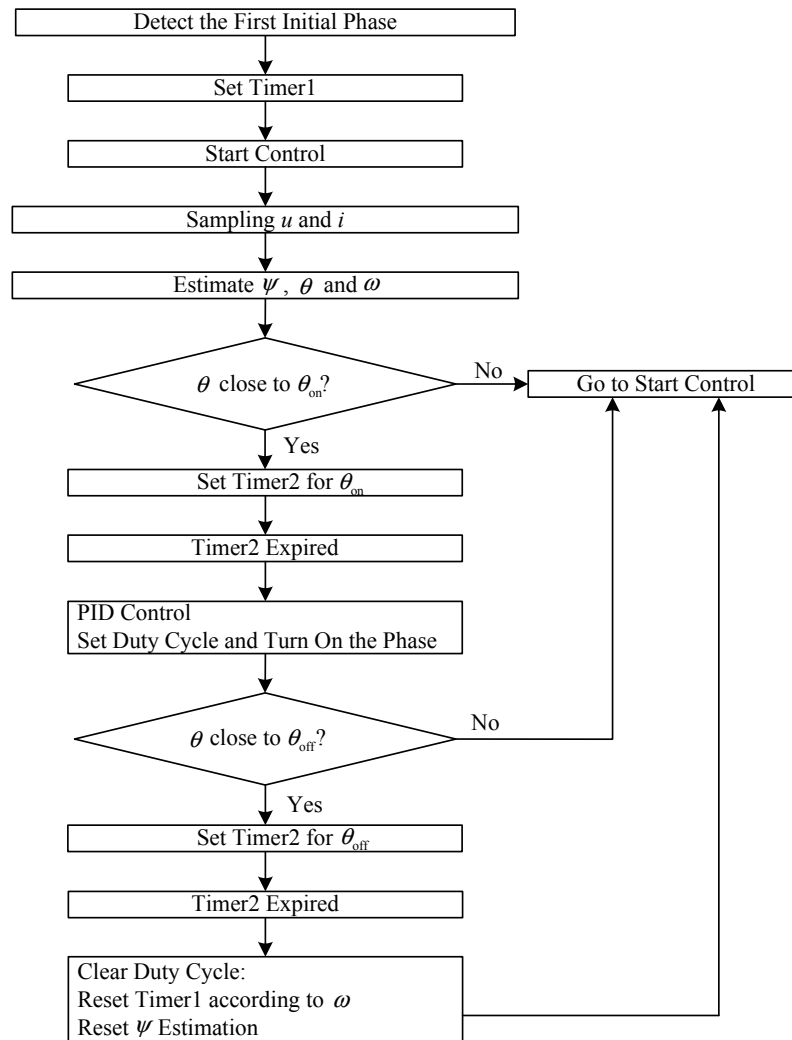
Figure 5. Flowchart of control algorithm.

5.2. PSO-RVM-Based Estimation Model Training

Parameters of the prototype three-phase 12/8 structure SRM are given in Table 1, with the prototype SRM's rated power of 2 kW, rated RPM of 3000 r/min, rated voltage of 110 V and rotary inertia of 0.008 kg·m². Considering the instable open-loop control of SRM, the training and test sample sets were both obtained under closed-loop control. To ensure that the sampled data could cover the non-linear characteristic of the SRM flux-linkage, the overload coefficient in practical operation of SRM was also used to determine the range of winding current detection: 0 A~20 A. Through testing, 500 sample sets were obtained and the sampled data were processed by means of normalization by decimal scaling. Among the 500 sample sets, 300 were selected to be the training sample sets for offline training of the PSO-RVM-based rotor position estimation model while the other 200 were used as test sample sets to examine the estimation precision of the model.

In offline training, the initial values of α were set as follows: $\alpha_i = 0.1$, $\sigma^2 = 0$, convergence condition of the RVM algorithm: $|\ln \alpha - \ln \alpha_{\text{new}}| < 10^{-6}$, number of particles: 30, number of circulation: 100, minimum adaptive threshold: $f_{\min} = 1 \times 10^{-6}$, inertia weight ω ranging from 0.45 to 0.95 along

with the linear increase of circulating number, learning factor $c_1 = c_2 = 2.05$, iterative initial value $\delta^2 = 46.1$ based on empirical selection and the δ^2 optimization space as [0.01, 100] [21,22].

Table 1. Partial specification of SRM.

Parameters	Value
Stator outer diameter (mm)	110
Stator inner diameter (mm)	54
Rotor outer diameter (mm)	53.4
Rotor inner diameter (mm)	34
Air gap (mm)	0.3
Stator/rotor pole arc (°)	15
Number of phases	3

5.3. PSO-RVM-Based Estimation Model Evaluation

To examine the effectiveness of PSO-RVM in building the SRM rotor position estimation model, a comparative analysis among PSO-RVM, RVM and SVM was performed and the kernel function parameters δ^2 of the RVM and SVM were obtained through GA. The maximum absolute error ε_{mae} and the mean absolute percentage error ε_{MAPE} were adopted as performance indicators to measure the model's precision. These indicators are defined as:

$$\varepsilon_{mae} = \max_j \left| y_j' - y_j \right| \tag{21}$$

$$\varepsilon_{MAPE} = \frac{1}{n} \sum_{j=1}^{n} \left| \frac{y_j' - y_j}{y_j'} \right| \times 100\% \tag{22}$$

where y_j' represents the predictive value and y_j denotes the actual value.

With the same training and test sample sets, the performance indicators of the PSO-RVM, RVM and SVM algorithms, such as the kernel function parameter δ^2, ε_{mae}, ε_{MAPE}, number of vectors and time of decision making, are listed in Table 2, wherein RVs and SVs represent the number of relevance vectors and the number of support vectors, respectively.

Table 2. Compare of PSO-RVM, RVM and SVM. SVM: support vector machine

Parameter	PSO-RVM	RVM	SVM
δ^2	4.12	3.25	6.79
ε_{mae} (°)	0.11	0.83	1.32
ε_{MAPE} (%)	0.025	0.06	0.172
RV_S/SV_S	5	5	23
Time (ms)	0.15	0.15	1.84

From Table 2, it is found that:

(1) The optimal kernel function parameter δ^2 of PSO-RVM and that of RVM given by the PSO algorithm and GA differ from each other. Since these optimization algorithms are subject to different principles, it is difficult to compare the corresponding optimization results. Yet, the ε_{mae} and ε_{MAPE} values produced by the PSO-RVM model are both smaller than those of the RVM model, showing that the PSO algorithm outperforms GA in searching optimal kernel function parameter.

(2) The ε_{mae} and ε_{MAPE} values given by the PSO-RVM and RVM models are smaller than those of the SVM model because the SVM model builds a learning machine in the principle of structural risk minimization and thus the learning machine only allows dependency acceptance or rejection.

In contrast, the Bayes' theorem is applied to RVM for probabilistic forecasting, which enables quantitative evaluation of the dependency of test results. Therefore, the RVM method, compared to SVM, has a higher degree of likelihood precision and greater generalization performance in training sampled data.

(3)   The number of relevance vectors of the SVM model is 3–4 times more than that of the PSO-RVM model and the RVM model respectively. Because the number of relevance vectors (support vectors) determines the computation speed in the decision-making stage of a model, the decision making of the RVM method is shorter than that of SVM, which suggests that the results produced by the RVM method show a higher level of sparsity and the model has a simpler structure and shorter online computation. In general, RVM is more suitable for SRM at high speed operation.

5.4. Real-Time Estimation Effects

As to the SRM parameters listed in Table 1, the 3D finite element simulation software Ansoft/Maxwell was used for building an SRM electromagnetic field model and carry out dynamic simulation study in the Matlab/Simulink environment.

Figure 6a presents a comparison between the actual and estimated SRM rotor positions at 3000 r/min while Figure 6b records the rotor position estimation error. It can be seen that, at 3000 r/min, the maximum estimation error is $360° \times 0.011 \text{ rad}/2\pi = 0.63°$. The minor error will not affect the phase inversion of SRM.
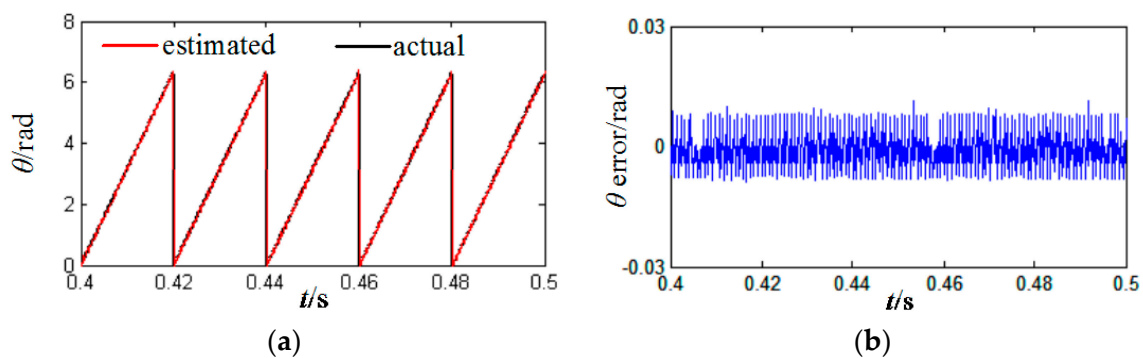
Figure 6. Rotor position simulation at 3000 r/min. (**a**) The actual angle and the estimated angle; (**b**) Estimation error.

When $t = 0.7$ s, the disturbance torque of 0.25 Nm is added and the SRM torque-RPM response curve is shown in Figure 7. According to Figure 7, under the circumstance of sudden load disturbance, the motor still maintains steady operation at the given RPM and torque output promptly increases with slight pulsation, which verified the stability of the control system.
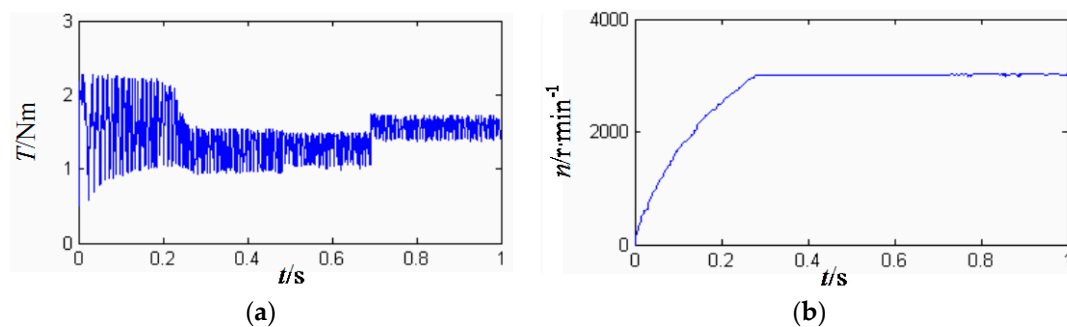
Figure 7. Simulation results of sudden load change of 0.25Nm at 3000 r/min. (**a**) Torque; (**b**) Speed.

5.5. Experiment

The SRM rotor position self-sensing control system is as shown in Figure 8, which is comprised of a power converter, a digital signal processing (DSP) control and drive circuit, a voltage-current detector, a motor and a protective circuit. Particularly, insulated gate bipolar transisor (IGBT) is set as the main switch of the power converter; the TMS320F28335 chip of the DSP is provided by Texas Instruments, which enables sampling of voltage, current and angular signals, flux-linkage estimation, RVM model training, rotor position identification, motor control algorithm and PWM signal output. In Figure 8, ADC is the analog to digital converter and SCI is the serial peripheral interface. During experiment, a rotor-position sensor was installed to detect the actual rotor position and improve the verification of the effectiveness of the PSO-RVM estimation model by comparing the PSO-RVM estimated rotor position with the actual rotor position.
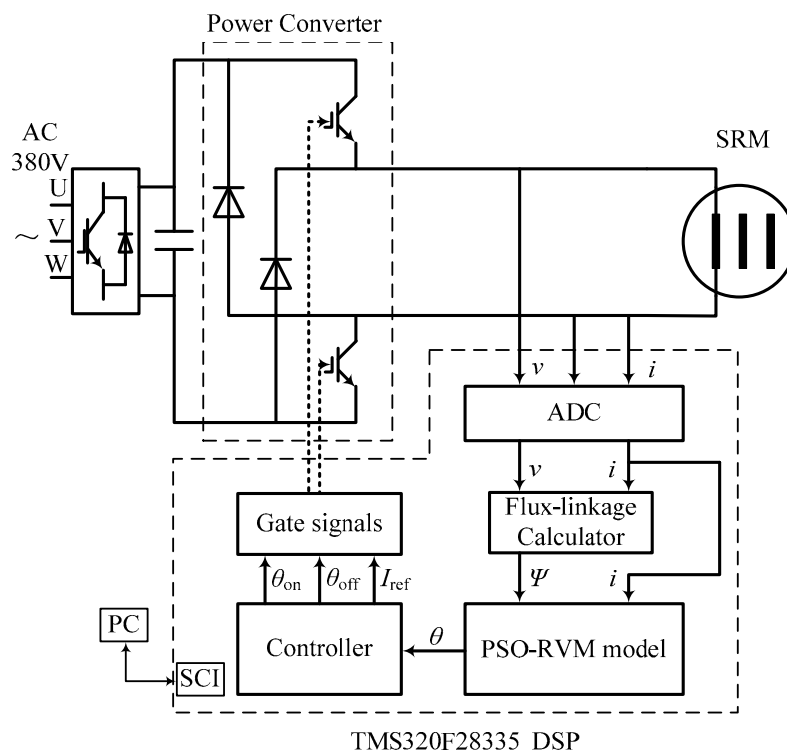
Figure 8. The experiment control block diagram

Figure 9a shows the operation curve of the protocol at 1500 r/min under chopped current control, where the current and voltage are actual values, the flux-linkage is the DSP calculation result and the angle is a predictive value given by the PSO-RVM model; Figure 9b presents the PSO-RVM estimated rotor position angle, actual rotor position angle through detection with sensors and estimation error, where the maximum system position error is 1.3°. With the same experimental methods, the operation curve and estimation error when the protocol is at 3000 r/min and under angular position control are shown in Figure 10a,b where the maximum system position error is 1.7°. The experimental results with the protocol at varied RPMs and under control by different methods suggest that the PSO-RVM-based rotor position self-sensing method shows a high degree of detection precision and allows SRM position sensorless control.
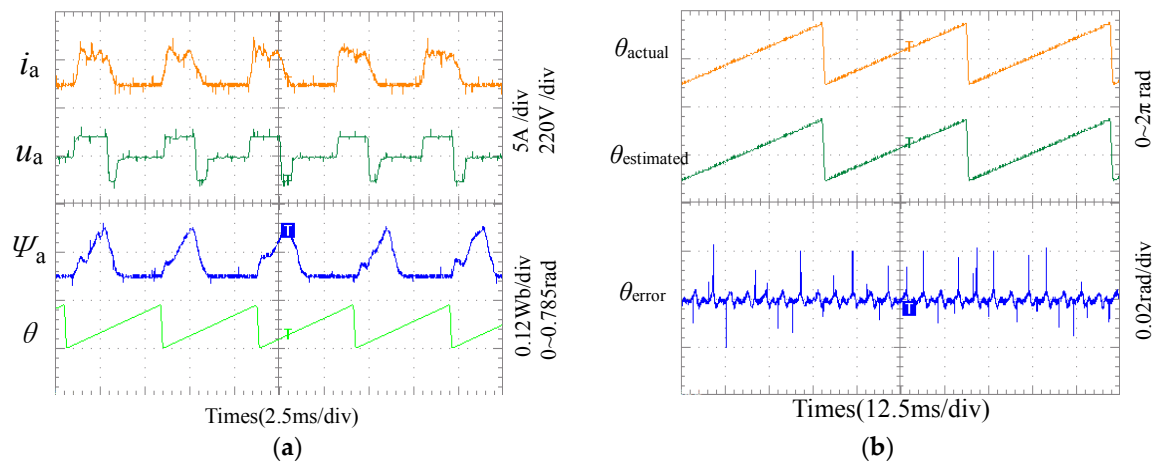
Figure 9. Experiment results at 1500 r/min. (**a**) Measured phase current, phase voltage and estimated flux-linkage, rotor angle; (**b**) Actual, estimated rotor position and error.
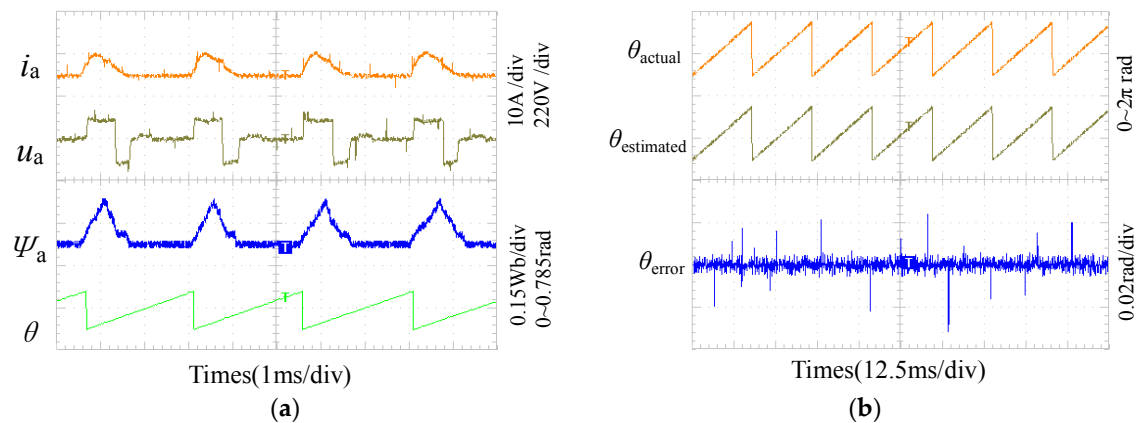
Figure 10. Experiment results at 3000 r/min. (**a**) Measured phase current, phase voltage and estimated flux-linkage, rotor position; (**b**) Actual, estimated rotor position and error.

6. Conclusions

This paper realized SRM rotor position self-sensing by using PSO-RVM as a learning machine, building an SRM rotor position non-linear estimation model and implementing rotor position estimation. With the optimized kernel function parameter in RVM, the PSO-RVM model can predict the rotor position more accurate than conventional RVM model. And the proposed method has a shorter on-line testing time compared with the SVM and NN self-sensing, which makes the motor operating in higher speed such as 3000 r/min. Moreover, the PSO-RVM model can obtain continuous rotor angle in the full cycle, so the motor can be operated in both current chopped control and angle position control. Finally, the SRM rotor position self-sensing control system is built by DSP. The simulation and experimental results verify the effectiveness of the proposed method.

Author Contributions: Qianwen Xiang proposed control method and performed simulation analysis and drafted the manuscript, Ye Yuan tested control software and designed hardware system, Yanjun Yu did the finite element simulation, Kunhua Chen did the experiment.

Conflicts of Interest: The authors declare no conflict of interest.

References

1. Kuai, S.Y.; Rallabandi, V.; Ionel, D.M. Sensorless control of three phase switched reluctance motor drives using an approximate inductance model. In Proceedings of the IEEE International Electric Machines and Drives Conference, Miami, FL, USA, 21–24 May 2017; pp. 1–6.
2. Ehssai, M.; Husaln, I.; Kulkami, A.B. Elimination of discrete position sensor sad current in switched reluctance motor drives. *IEEE Trans. Ind. Electron.* **1992**, *28*, 128–135.
3. Ofori, E.; Husain, T.; Sozer, Y.; Husain, I. A pulse-injection-based sensorless position estimation method for a switched reluctance machine over a wide speed range. *IEEE Ind. Appl. Soc.* **2015**, *51*, 3867–3876. [CrossRef]
4. Li, P.; Zhang, L.; Yu, Y. A novel sensorless for switched reluctance motor based on sliding mode observer. In Proceedings of the Electronic and Automation Control Conference, Chongqing, China, 25–26 March 2017; pp. 1560–1564.
5. Konrad, U.; Krzysztof, Z. Sensorless control of SRM using position observer. In Proceedings of the European Conference on Power Electronics and Applications, Aalborg, Denmark, 2–5 September 2007; pp. 1–6.
6. Gallegos-Lopez, G.; Kjaer, P.C.; Miller, T.J. High grade position estimation for SRM drives using flux linkage/current correction model. *IEEE Trans. Ind. Appl.* **1998**, *34*, 859–869.
7. Zhang, L.; Liu, C.; Wang, Y.L.; Zhang, Y.L. Sensorless technology of switched reluctance motor based on the improved simplified flux method. *Electr. Mach. Control* **2013**, *17*, 13–19.
8. Li, Z.G.; Li, C.H.; Kan, Z.Z.; Zhang, C. Switched reluctance motor sensorless speed control based on the improved simplified flux method. *Trans. China Electrotech. Soc.* **2011**, *26*, 62–66.
9. Wang, J.J.; Sun, J.H.; Zheng, Z.Y. Position Control of SRM based on sliding-mode-learning neural networks. *Control Decis.* **2017**, *32*, 1133–1136.
10. Polat, M.; Oksuztepe, E.; Kurum, H. Switched reluctance motor control without position sensor by using data obtained from finite element method in artificial neural network. *Electr. Eng.* **2016**, *98*, 43–54. [CrossRef]
11. Zhong, R.; Xu, Y.Z.; Cao, Y.P.; Guo, X.; Hua, W.; Xu, S.; Sun, W. Accurate model of switched reluctance motor based on indirect measurement method and least square support vector machine. *IET Electr. Power Appl.* **2016**, *10*, 916–922. [CrossRef]
12. Zhong, R.; Wang, Y.B.; Xu, Y.Z. Position sensorless control of switched reluctance motors based on improved neural method. *IET Electr. Power Appl.* **2012**, *6*, 111–121. [CrossRef]
13. Wang, J.J. Adaptive inverse position control of switched reluctance motor. *Appl. Soft Comput. J.* **2017**, *60*, 48–59. [CrossRef]
14. Saravanan, P.; Balaji, M.; Arumugam, R. Analysis of neural network approaches for nonlinear modeling of Switched Reluctance Motor drive. *J. Electr. Eng. Technol.* **2017**, *12*, 1548–1555.
15. Song, S.S.; Ge, L.F.; Zhang, M. Data-Reconstruction-Based Modeling of SRM with Few Flux-Linkage Samples from Torque-Balanced Measurement. *IEEE Trans. Energy Convers.* **2016**, *31*, 424–435. [CrossRef]
16. Tipping, M.E. Sparse Bayesian learning and relevance vector machine. *J. Mach. Learn. Res.* **2001**, *1*, 211–244.
17. Tipping, M.E. The relevance vector machine. *Adv. Neual Inf. Process. Syst.* **2000**, *12*, 652–658.
18. Tzikas, D.G.; Likas, A.C.; Galatsanos, N.P. Sparse bayesian modeling with adaptive kernel learning. *IEEE Trans. Neural Netw.* **2009**, *20*, 926–937. [CrossRef] [PubMed]
19. He, S.M.; Xiao, L.; Wang, Y.L.; Liu, X.; Yang, C.; Lu, J.; Gui, W.; Sun, Y. A novel fault diagnosis method based on optimal relevance vector machine. *Neurocomputing* **2017**, *267*, 651–663. [CrossRef]
20. Jin, X.; Hui, X.F. Financial assets price prediction based on relevance vector machine with genetic algorithm. *J. Converg. Inf. Technol.* **2012**, *7*, 90–96.
21. Eber, R.C.; Shi, Y. Comparing inertia weights and constriction factors in particle swarm optimization. In Proceedings of the 2000 Congress on Evolutionary Computation, La Jolla, CA, USA, 15–17 July 2000; pp. 84–88.
22. Wang, D.F.; Meng, L. Performance Analysis and Parameter Selection of PSO Algorithms. *Acta Autom. Sin.* **2016**, *42*, 1552–1561.